# Mode analysis and design of 0.3-THz Clinotron*

Shuang Li(李爽)[1,2], Jian-Guo Wang(王建国)[1,2,†], Guang-Qiang Wang(王光强)[2], Peng Zeng(曾鹏)[2], and Dong-Yang Wang(王东阳)[2]

[1] *Key Laboratory for Physical Electronics and Devices of the Ministry of Education, Xi'an Jiaotong University, Xi'an* 710049, *China*
[2] *Laboratory on Science and Technology of High Power Microwave, Northwest Institute of Nuclear Technology, Xi'an* 710024, *China*

(Received 24 April 2016; revised manuscript received 31 May 2016; published online 25 August 2016)

To develop a high-power continuous-wave terahertz source, a Clinotron operating at 0.3 THz is investigated. Based on the analyses of field distribution and coupling impedance, the dispersion characteristic of a rectangular resonator is preliminarily studied. The effective way to select fundamental mode to interact with the electron beam is especially studied. Finally, the structure is optimized by particle-in-cell simulation, and the problems of manufacture tolerance, current density threshold, and heat dissipation during Clinotron's operation are also discussed. The optimum device can work with a good performance under the conditions of 8 kV and 60 mA. With the generation of signal frequency at 315.89 GHz and output power at 12 W on average, this device shows great prospects in the application of terahertz waves.

**Keywords:** terahertz, Clinotron, mode selection, particle simulation

**PACS:** 84.40.Fe, 45.10.Db, 52.65.–y **DOI:** 10.1088/1674-1056/25/10/108401

## 1. Introduction

In order to develop the potential applications of terahertz waves in space communication, high resolution radar and so on, it is crucial to develop the terahertz source with high output power first. In the low frequency band of terahertz, several kinds of vacuum electronic devices (VEDs) can generate continuous wave or pulsed wave with high output power,[1,2] one of which—Clinotron—has the capability of increasing the beam-wave interaction efficiency and output power as well,[3–12] showing promising prospects in the development of a terahertz source. The most famous research organization of Clinotron is the National Academy of Sciences (NAS) of Ukraine. As reported in Ref. [13], one type of Clinotron can work at 345 GHz–390 GHz and an output power of about 100 mW. Its working current reaches as high as 160 mA. Another type of "Clinotron-0.95" can work at 272 GHz–334 GHz with an output power in a range of 50 mW–100 mW as reported.[11]

Due to the unique feature of transferring the energy of an electron beam into the strong surface electric field, Clinotron can greatly improve the efficiency of interaction. What is more, the use of sheet electron beam provides the advantage that each layer of electron beam can interact with electric field sufficiently to raise the output power.[13] However, there are also many problems during the research of Clinotron, such as the mode competition in the rectangular resonator, the precise magnetic field system, and the heat dissipation in metal.

Based on the theoretical analysis of Clinotron and the research of field distribution and coupling impedance, the mode selection in Clinotron is studied in depth. The design of Clinotron structure is optimized by the particle-in-cell (PIC) simulation and the related physical processes are also discussed.

## 2. Theoretical analysis

The configuration of Clinotron is shown in Fig. 1. The rectangular comb is used as the slow wave structure (SWS).

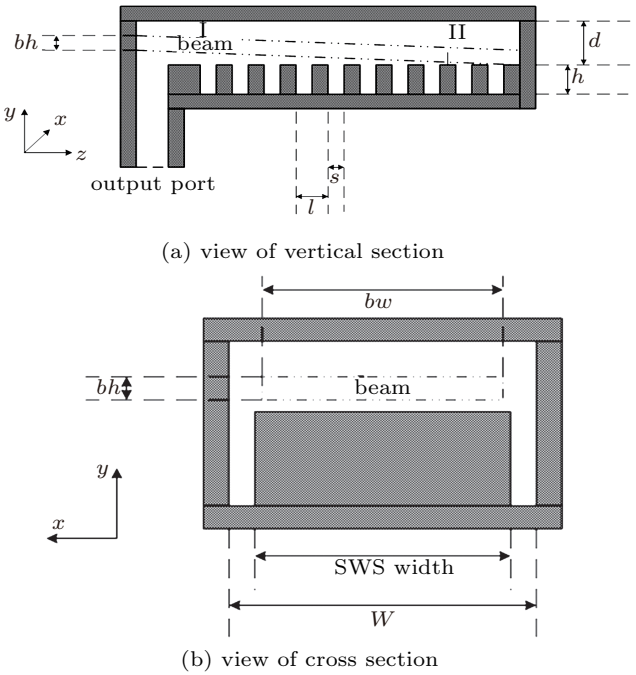



**Fig. 1.** Views of (a) vertical section and (b) cross section of Clinotron ('*bh*' denotes the beam thickness, '*bw*' the beam width, '*l*' the period length of SWS, '*s*' is the width of comb-gap, '*d*' denotes the distance between comb and top, '*h*' is the depth of a comb, '*W*' the width of cavity.)

*Project supported by the National Natural Science Foundation of China (Grant No. 61231003).
†Corresponding author. E-mail: wanguiuc@mail.xjtu.edu.cn
© 2016 Chinese Physical Society and IOP Publishing Ltd 

### 2.1. Dispersion

It is very difficult to find an exact way to express the dispersion of the closed resonator with periodic rectangular comb. An approximate method is usually used to study such a structure. The whole cavity is divided into two regions, named I and II, which are studied by applying different boundary conditions. Under the supposition of $l \ll \lambda_0$ ($\lambda_0$ is the wavelength in space), the high-order harmonic waves can be ignored in region I and there is only TEM wave propagating toward the $y$ direction.[14,15] The fields in region II can be considered as TM modes which contain the components of $E_y$ and $E_z$.

Combining with the electric fields in two parts on the borders of I and II, the dispersion relationship in this cavity can be obtained as[16–18]

$$\begin{aligned} & \nu_0 l \tanh(\nu_0(b-h))\cos(\nu_x h) \\ = \; & \nu_x l \sin(\nu_x h)\mathrm{sinc}^2\left(\frac{k_{z0}s}{2}\right)\frac{s}{l} + \nu_0 l \tanh(\nu_0(b-h))\nu_x l \\ & \times \sin(\nu_x l)\frac{s}{l}\sum_{n=-\infty,n\neq 0}^{\infty}\frac{\mathrm{sinc}^2(k_{zn}s/2)}{\nu_n l \tanh(\nu_n(b-h))}. \end{aligned} \tag{1}$$

### 2.2. Coupling impedance

The coupling impedance is used to describe the interaction of beam and axial electric field. It is expressed as

$$K_p^{(n)} = \frac{|E_z^{(n)}|^2}{2(\beta_z^{(n)})^2 \Pi}, \tag{2}$$

where $\beta_z^{(n)} = k_{zn}$ denotes the transmission constant of the $n$-harmonic wave, and the parameter $\Pi$ denotes the sum of powers of all harmonic fields in the cavity.[19]

### 2.3. Mode distribution in rectangular resonator

The electric fields distributed in a Clinotron resonator are recognized to be in $\mathrm{TM}_{mp}$ mode, where the subscripts of $m$ and $p$ indicate the numbers of half wave distribution along the $x$ and $y$ directions, respectively.[20,21] The field distribution of $E_z$ with $\mathrm{TM}_{10}$ mode, the fundamental mode, is computed theoretically, and the results are shown in Fig. 2. It is clear that $E_z$ behaves as a standing wave along the $z$ direction and attenuates along the $y$ direction. The field near the surface of SWS is strongest, which means the field here can interact with the electron beam most effectively. The coupling impedances of different modes are computed to compare the influences of field distributions on the beam–wave interaction, which are given in Fig. 3.

It is obvious that the biggest coupling impedance occurs near the surface of SWS for $\mathrm{TM}_{m0}$ ($m \neq 0$) mode. The value of impedance drops rapidly with the distance increasing to SWS, so it is crucial to keep the electron beam as close to SWS as possible. Moreover, the range of impedance along the $x$ direction is associated with the field distribution. The range of

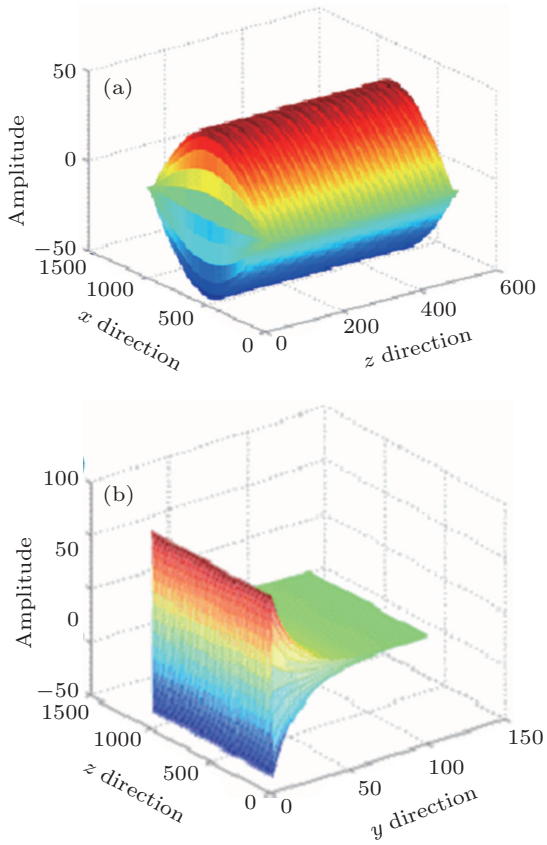



**Fig. 2.** (color online) Distributions of $E_z$ in $\mathrm{TM}_{10}$ mode for the (a) $xz$- and (b) $yz$-section view.

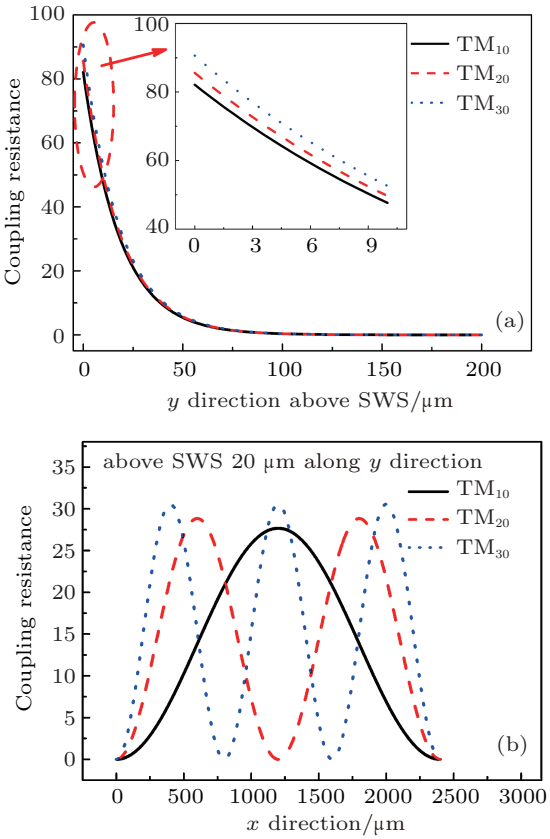



**Fig. 3.** (color online) Coupling impedances of different modes in (a) $y$ direction and (b) $x$ direction.

the fundamental wave is widest and that of the high-order harmonic waves are narrow correspondingly. Though the peak values of the high-order harmonic waves are comparatively high, the ranges are really narrow, which do not match the wide spread sheet beam very well. As a result, it is suggested to make sure that the beam can interact with the $TM_{10}$ mode but not with other high modes. Then, the advantage of sheet beam can be fully exploited and the output power can be improved.

## 3. Mode selection

Actually, there will be many modes existing in a cavity at the same time, which include the high-order harmonic modes along not only the $x$ direction but also the $y$ direction, such as $TM_{20}$, $TM_{22}$, etc. The presence of high harmonic fields is really harmful to the device efficiency as indicated above. The fundamental mode is required to be excited as a main mode in the cavity and the other high modes are expected to be suppressed.[22,23] In order to distinguish different modes, the dispersion relations are analyzed in Fig. 4.

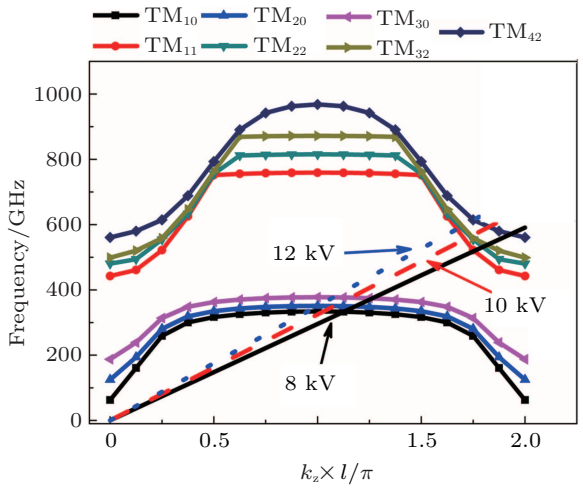



**Fig. 4.** (color online) Dispersion curves of different modes in Clinotron cavity.

Since there are distinct spaces between fundamental mode and the high modes of $p \neq 0$ ($TM_{11}$ and $TM_{22}$), such kinds of high-order modes are easy to pick off. The keen competitions come from other kinds of high modes that are $p = 0$ ($TM_{20}$ and $TM_{30}$). The proposed method here is to select the mode by designing structure parameters and adjusting the beam voltage at the same time. As to the beam voltage, the principle for selection is to adjust the working point to locate near the $\pi$-point of $TM_{10}$ mode and to keep away from the $\pi$-point of other modes. The reason is that the group velocity is close to zero near $\pi$-point and the $Q$ value of this mode is rather high, which both lead to small starting current for $TM_{10}$ mode. As can be seen in Fig. 4, there are three beam lines respectively for the beam voltages of 8 kV, 10 kV, and 12 kV, and they match modes at different points. Obviously, the line of 10 kV is much closer to the $\pi$-point of $TM_{10}$ mode and far from $\pi$-points of $TM_{20}$ and $TM_{30}$ modes. So the device will work easily at $TM_{10}$ mode when the beam is 10 kV and the other modes can be avoided. If the voltage is much higher, say, 12 kV, this beam line will successfully cross $TM_{20}$ mode at $\pi$-point and leave away from the $\pi$-point of $TM_1$ mode. The device will more likely oscillate at $TM_{20}$ mode, which is unexpected. On the other hand, the shapes of dispersion curves under different parameters are different. Referring to the influence of SWS periodic length ($l$) on dispersion in Fig. 5, it can be found that at the same working point, the distance among each of the modes of $l = 0.1$ mm is larger than that of $l = 0.5$ mm. The smaller the value of periodic length, the flatter the dispersion curve will be. By setting a small value of $l$, the gaps among modes are large so that the working points of high-order harmonic modes are far away from the $\pi$-point, which is of benefit to the fundamental mode to be excited first.

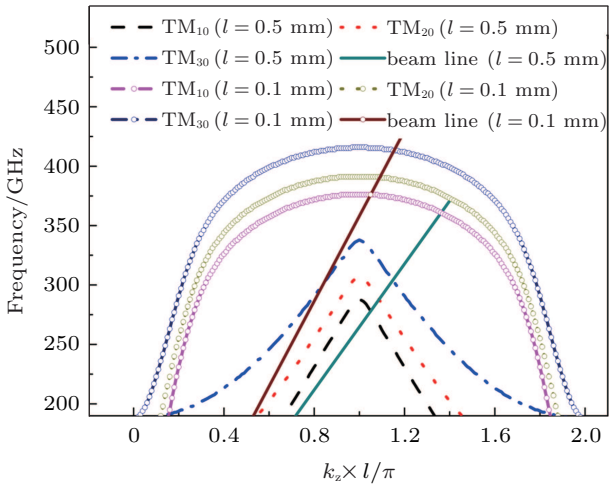



**Fig. 5.** (color online) Influences of periodic length on dispersions for different modes.

Furthermore, different modes need different starting currents to oscillate in the resonator. The point near $\pi$-phase of $TM_{10}$ mode has priority to be excited. As the current increases, many other modes will be excited in the cavity. Figure 6 shows the results of modes in the cavity under different current densities, obtained by particle-in-cell (PIC) simulation.

More high-order harmonic modes will appear with the increase of current density. As shown in Fig. 6, $TM_{10}$ mode (319 GHz) is first to be excited and it is the only mode existing in the cavity when the current density is smaller than 35 A/cm$^2$. Once the current density is larger than 35 A/cm$^2$, $TM_{20}$ mode (363 GHz) will be excited in the cavity. If the current keeps increasing, the $TM_{30}$ mode (432 GHz) will also appear at the same time. The results in Fig. 6 illustrate that it is

feasible to realize the selection of only $TM_{10}$ mode in the cavity by finding the starting current requirements and working at the advised parameters.

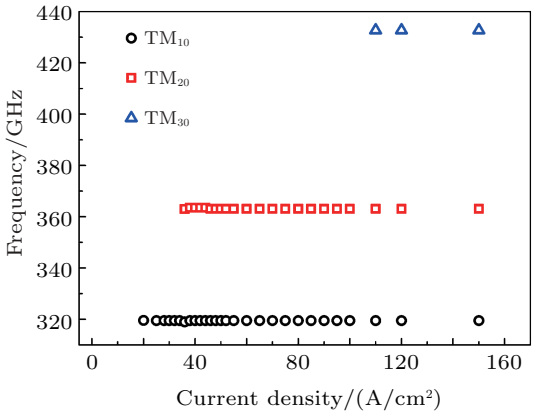



**Fig. 6.** (color online) Influences of current density on the oscillation for different modes in cavity.

## 4. Optimum design

### 4.1. Beam voltage

The results of output power, frequency, and starting time under different beam voltages are compared in Fig. 7.

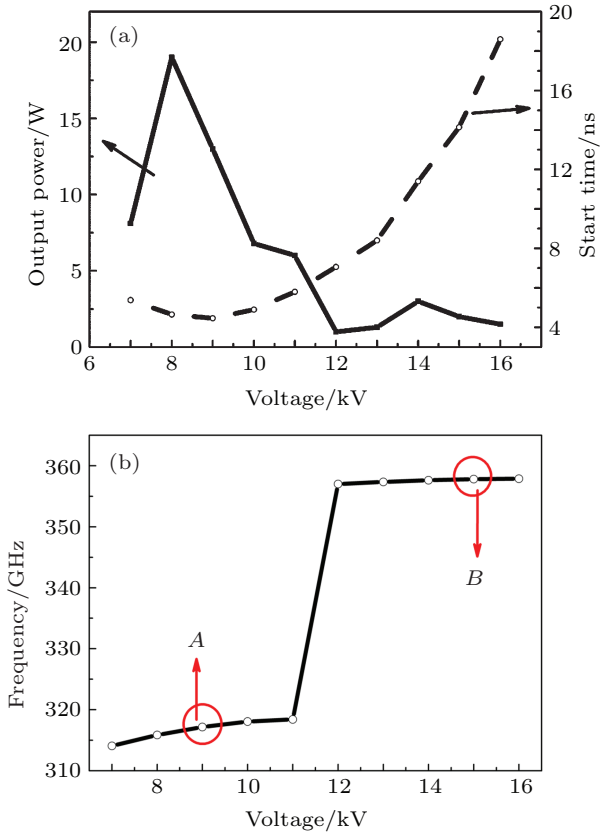



**Fig. 7.** (color online) Influences of beam voltage on (a) output power and starting time, and (b) signal frequency

Beam voltage determines the device working point on the dispersion curve. Based on the results of theoretical dispersion curve, the range from 8 kV to 10 kV is confirmed to make the beam interact with the backward wave of $-1$ order harmonic. The choices of these working points ensure a higher output power and shorter starting time as shown in Fig. 7(a). As a rule, the shift of beam voltage will always bring the beam into interacting with high-order harmonic wave not fully with the fundamental wave. Once the voltage meets the condition of high order harmonic wave well, the beam energy will be sufficiently exchanged into the high harmonic wave and the performance of the device will change disappointingly. Just as shown in Fig. 7(b), the increase of beam voltage causes the working point to change from backward-wave area of fundamental mode to that of high-order mode, and the frequency of output signal is changed. According to the further analysis of PIC simulation results, the distributions of $E_z$ for points $A$ and $B$ in Fig. 7(b) are shown in Fig. 8. It is obvious that the device is working at $TM_{10}$ mode when the beam voltage is about 8 kV–10 kV, which is exactly the fundamental mode in the resonator. Meanwhile, with the increase of voltage, the distribution of point $B$ becomes $TM_{20}$ mode, the second high order mode in the resonator. Therefore, in order to acquire high efficiency and output power, the beam voltage should be accurately optimized to match the dispersion characteristic of the resonantor.

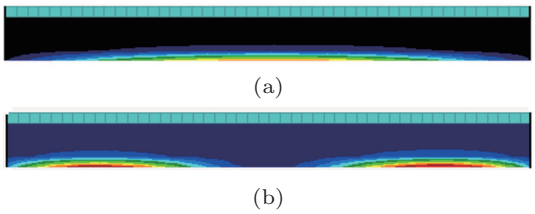



**Fig. 8.** (color online) Distributions of $E_z$ in (a) $TM_{10}$ mode corresponding to point $A$ in Fig. 7(b), and (b) $TM_{20}$ mode corresponding to point $B$ in Fig. 7(b).

### 4.2. Limitation of space charge field

As the source of energy, the amplitude of beam current plays an important role in determining the output power, and the results under different currents are compared with each other in Fig. 9.

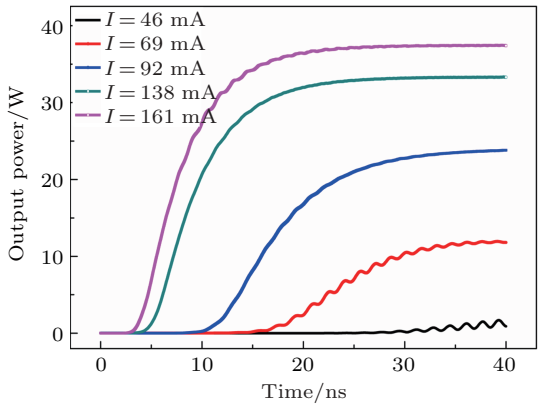



**Fig. 9.** (color online) Variations of output power with time for different currents.

High current will bring a comparatively good output result, which is clearly shown in Fig. 9. Meanwhile, the starting time for oscillation decreases. Under the condition of 69 mA, corresponding to the current density of 19 A/cm$^2$, the output power is about 10 W. When the current is doubled, i.e., 138 mA, the output power reaches 30 W, which is three times as great as the former output power. However, the output power cannot grow forever by increasing current because of the limitation from space charge field at the maximal current density.

The maximum of interaction distance can be described as[24,25]

$$l_{\mathrm{chr}} = \frac{1}{k_{\mathrm{sh}} \sin\alpha}, \tag{3}$$

where $k_{\mathrm{sh}} \approx \omega/v_0$ in Clinotron. Commonly, the space charge field can be ignored as long as the condition of $l_{\mathrm{chr}} \leq \lambda_p/2$ is satisfied. Based on the theory of space charge wave, the wavelength of plasma in the device can be expressed as $\omega_p = \sqrt{(e/m)(\rho_0/\varepsilon_0)}$, where $\rho_0 = J_0/v_0$ is the charge density and it is the only factor that determines the plasma wavelength. Using the above formulas, the maximum current allowable in the cavity can be described as

$$J_{0\max} = \frac{\pi^2 \varepsilon_0 m v_0 \omega^2}{|e|} \sin^2\alpha, \tag{4}$$

where $\omega$ is the angular frequency.

Supposing that the working frequency is 310 GHz, the maximum current densities are computed for different beam voltages and inclined angles and the results are shown in Fig. 10.

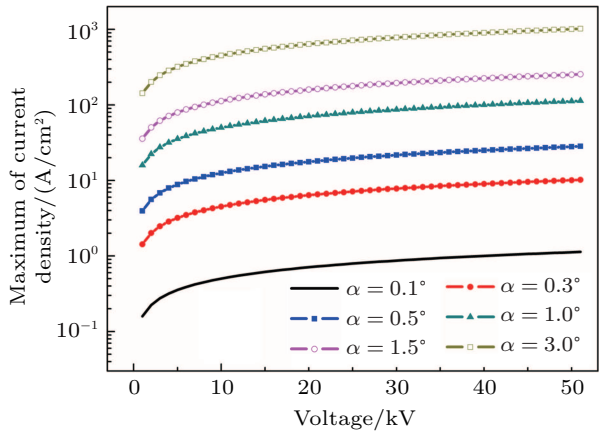



**Fig. 10.** (color online) Variations of maximum current density with voltage at different inclined angles.

It can be seen in Fig. 10 that the threshold of current density does not change greatly at the same inclined angle when the beam voltage changes, but a bigger inclined angle could realize the improvement of threshold. By comparing the results of 1.0° and 0.1°, the threshold is improved ten times under the same voltage of 10 kV. The influence of inclined angle is actually related to the effect of space charge. The equivalent current near SWS surface is rather strong under the condition of a small angle, which leads to stronger effect of space charge. On the contrary, when the angle is big, the limitation from space charge is weakened and thus the threshold would be improved. Figure 11 shows the output results at different inclined angles and here the values of current density are all chosen to be 25 A/cm$^2$.

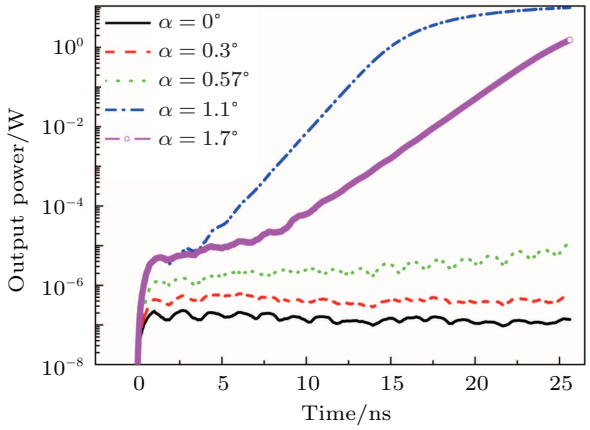



**Fig. 11.** (color online) Variations of output power with time at different inclined angles.

As shown in Fig. 11, when the beam goes straight along SWS, the interaction process is badly affected because of the strong power from the space charge wave. The low values of current density threshold under the condition of small angle restricts the interaction efficiency. Increasing the inclined angle is helpful in enlarging the threshold and avoiding the limitation from the space charge field. The output power increases rapidly with the introduction of larger inclined angle. However, when the working current density does not exceed the threshold, it is not suggested to go on increasing the angle. There are two reasons for this proposition. Firstly, a larger angle means a shorter distance for effective interaction from Eq. (3). The output power will then be reduced though the current is enough for the interaction, which is demonstrated from the results of $\alpha = 1.1°$ and $\alpha = 1.7°$ in Fig. 11. The other consideration is that the big inclined angle will cause some other troubles in heat diffusion. Thus, it is strongly suggested to consider both space charge limitation and the requirement of output power to make a balance in determining the inclined angle.

### 4.3. Feasibility analysis

#### 4.3.1. Manufacture technology

For VED in THz region, the microfabrication is significant for the device performance so that the common fabrication methods are not suitable any longer. Nowadays, the advanced methods mainly focus on LIGA (LIthographie, Gal-

vanik, und Abformung), deep reactive ion etching (DRIE), and wire electrical discharge machining (WEDM).

Considering the designed Clinotron above, the minimum scale in the structure is 0.05 mm which is the width of the comb-gap. This size is about ten times larger than the manufacture precision of WEDM, which could ensure the accuracy of specified configuration from the opinion of experience. What is more, the combs in Clinotron are all of regular rectangles without any complex shapes, thereby reducing the difficulties in achieving them. However, no manufacture is perfect and even a tiny tolerance may affect the device performance more or less. As discussed in Ref. [26], the parameters that could exert great effects on the device are the comb depth and the period length of SWS. The influences of SWS depth and period length on dispersion in this Clinotron have been investigated in Ref. [23]. As shown in this work, in this optimized Clinotron, the dispersion curve is comparatively flat and the shifts between adjacent dispersion curves under very close parameters are really small. Under the tuning voltages, the shift of working point caused by tolerance will not influence the performance intensively.

Thus, the optimized device manufactured by WEDM here is acceptable and the influence of tolerance is under control.

#### 4.3.2. Material

Commonly, the materials used in vacuum electron device are stainless steel, copper and gold. These metals are able to provide high power capabilities and good conductive characteristics, although, when the device works in a terahertz range, the precision of manufacture plays a significant role in determining its performance. The ability to account for the ohmic loss during the design stage is essential for properly optimizing the design parameters in order to achieve the desired performance. An estimate of the additional ohmic loss caused by surface roughness is fundamental for the proper structure. The surface roughness should be smaller than the skin depth ($\delta = \sqrt{2/(\omega\mu\varepsilon)}$) of the used metal, or else it may cause significant additional power loss. The skin depth of stainless steel is computed to be about 730 nm and the skin depths are 214 nm for copper and 17 nm for gold respectively. Thus, it is preferred to choose stainless steel in this device because the higher skin depth makes it much more promising in engineering realization.

#### 4.3.3. Heat dissipation

Besides the manufacture tolerance, the extreme high current will cause a lot of problems in experiment too. The heat will be accumulated in the SWS by electrons and then the material of SWS will be ruined, thereby destroying the steady state of the device. Hence the working current must be properly chosen from the viewpoint of heat dissipation. In Clinotron, the inclined beam usually strikes on the corner of the comb and the struck area is supposed to be as large as 1 μm×0.5 μm. Under the conditions of beam of 8 kV and 110 mA, the suffered energy storage can easily reach $E_\rho = 0.5 \times 10^4$ GeV/cm$^3$. Unfortunately, the threshold of stainless steel is about $0.7 \times 10^4$ J/cm$^3$, far smaller than the value of the above-assumed condition. So it is especially suggested that the current density of less than 30 A/cm$^2$ should be suitable and good for Clinotron. In the meantime, introducing the method of water-cooling to take the heat away is necessary. The working repetition frequency of the electron gun should be chosen to be about 50 Hz so that the water can have enough time to take the heat away.

#### 4.3.4. Inclined angle

As discussed above, a bigger inclined angle helps to improve the threshold of current density. However, an extremely big angle will also cause great energy of beam stuck on the SWS, which will affect the output results. Thus, the tradeoff value of angle should be analyzed in depth to ensure that the beam will not only meet the limitations from the space charge field and heat diffusion but also support the need of beam-wave interaction. When the working conditions are confirmed, it is convenient to design the inclined angle directly from formula (4). Based on the beam voltage of 8 kV and current density of 25 A/cm$^2$, the optimized inclined angle is computed to be 1.2°. This inclined beam is feasible and effective.

### 4.4. Optimized results

Based on the aforementioned research and the considerations on engineering feasibility, the optimized structure is finally summarized in Table 1 and the results from PIC simulation[27–29] are given in Fig. 12.

**Table 1.** Optimized structure of Clinotron.

| *bh*/mm | *bw*/mm | *l*/mm | *s*/mm | *h*/mm | *d*/mm |
|---|---|---|---|---|---|
| 0.1 | 2.4 | 0.1 | 0.05 | 0.2 | 0.2 |
| *W*/mm | SWS width/mm | voltage/kV | *J*/(A/cm$^2$) | *B*/T | $\alpha$/(°) |
| 2.6 | 2.6 | 8 | 25 | 0.6 | 1.1 |

In this simulation, beam voltage is set to be 8 kV and the current is 60 mA, which means that the current density is about 25 A/cm$^2$. The guiding magnetic field is 0.6 T and the inclined angle of beam is 1.1°. Consequently, the frequency of output wave is 315.89 GHz and the average output power is 12 W, corresponding to an efficiency of 2.5%. The choice of low current density ensures that the heat accumulated on material could be dissipated in time by water, guaranteeing the continuous-wave (CW) state of this device.

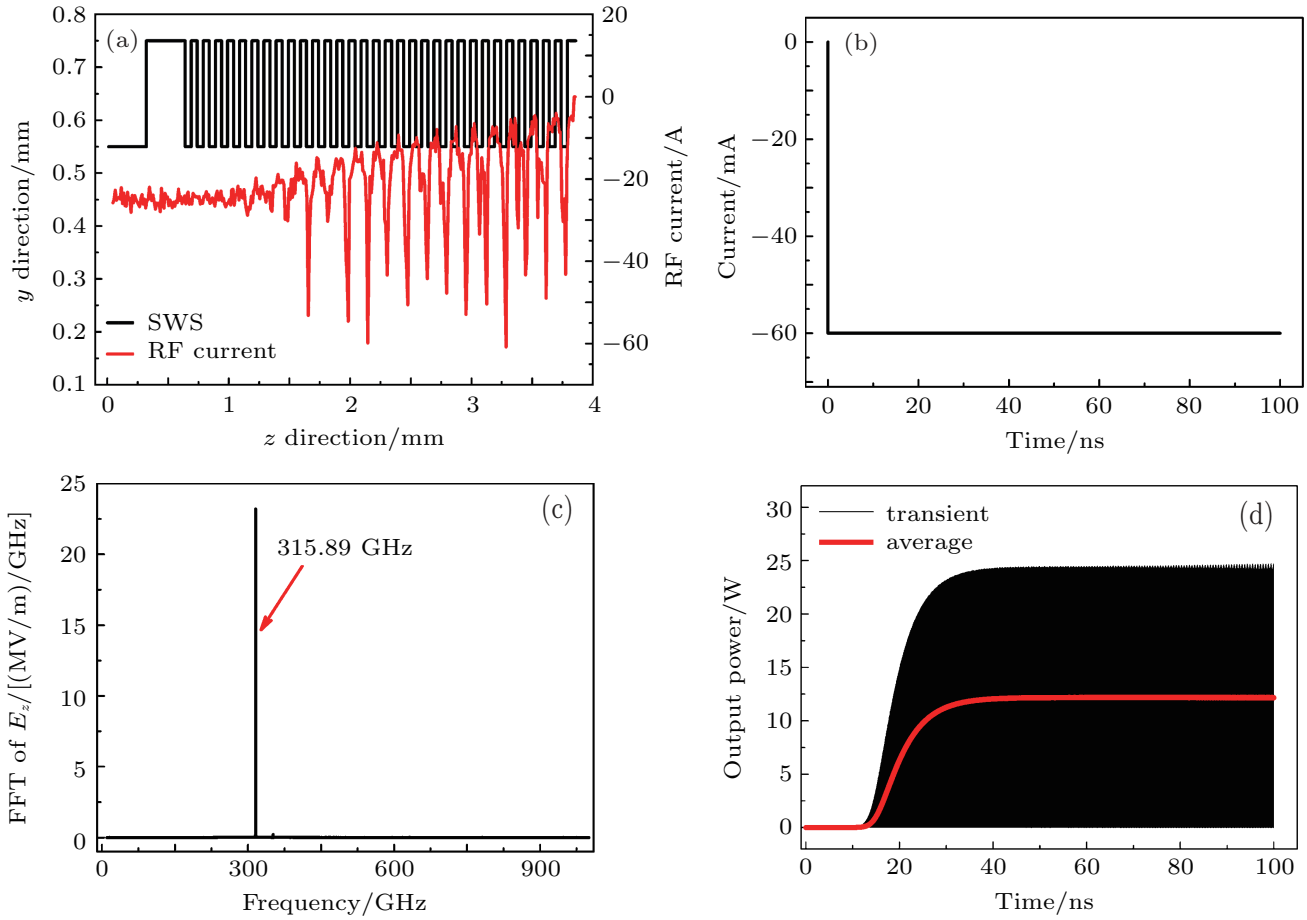



**Fig. 12.** (color online) Simulation results of optimum structure: (a) RF current and structure, (b) current, (c) FFT of $E_z$ at output port, and (d) output power.

## 5. Conclusions

Based on the interaction between beam and strong field near SWS surface, Clinotron is able to generate a considerable output power in THz region. The application of a sheet beam also helps to improve the efficiency of this device, making Clinotron a kind of potential oscillator generating terahertz waves. By analyzing the dispersion and coupling impedance, the field distributions of different modes in Clinotron are studied. The research emphases are the method of mode selection and the detailed conditions for operating at fundamental mode. The performance of Clinotron is analyzed by PIC simulation and the issues of manufacture tolerance, material selection, inclined angle and heat dissipation are also discussed theoretically. Finally, the optimum structure can work under the conditions of beam voltage of 8 kV, current of 60 mA and guiding magnetic field of 0.6 T, and it can reach a good and steady performance. Its output power is about 12 W on average and the frequency is 315.89 GHz.

## References

[1] Booske J H, Dobbs R J, Joye C D, Kory C L, Neil G R, Park G, Park J and Temkin R J 2011 *IEEE Trans. Terahertz Sci. Technol.* **1** 54

[2] Ren D and Feng J 2011 *Vacuum Electronics* **6** 21

[3] Wang G Q, Wang J G, Tong C J, Li X Z, Wang X F, Li S and Lu X C 2013 *Phys. Plasmas* **20** 043105

[4] Li X Z, Wang J G, Sun J, Song Z M, Ye H, Zhang Y C, Zhang L J and Zhang L G 2013 *IEEE Trans. Electron Dev.* **60** 2931

[5] Zhang K C and Wu Z H 2013 *Acta Phys. Sin.* **62** 024103 (in Chinese)

[6] Zhang K C, Qi Z K and Yang Z L 2015 *Chin. Phys. B* **24** 079402

[7] Chen Z G, Wang J G, Wang Y, Qiao H L, Guo W J and Zhang D H 2014 *Chin. Phys. B* **23** 068402

[8] Wang G Q, Wang J G, Li S, Wang X F, Lu X C and Song Z M 2015 *Acta Phys. Sin.* **64** 050703 (in Chinese)

[9] Sattorov M, Khutoryan E, Lukin K, Kwon O and Park G S 2013 *IEEE Trans. Electron Dev.* **60** 458

[10] Kim J I, Jeon S G, Kim G J, Kim J, Lopatin I V, Mil'cho M V and Tishchenko A S 2012 *Proceedings of the 37th International Conference on Infrared, Millimeter, and Terahertz Waves*, September 23–28, 2012, Wollongong, NSW, Australia

[11] Ponomarenko S S, Kishko S A, Zavertanniy V V, Khutoryan E M, Lopatin I V, Yefimov B P and Kuleshov A N 2013 *IEEE Trans. Plasma Sci.* **41** 82

[12] Ponomarenko S, Kishko S, Khutoryan E, Tishenko A, Kuleshov A and Yefimov B P 2012 *International Conference on Mathematical Methods in Electromagnetic Theory*, August 28–30, 2012, Kyiv, Ukraine, pp. 348–352

[13] Vavriv D M, Volkov V A and Chumak V G 2007 *Proceedings of the 37th European Microwave Conference*, October, 2007, Munich, Germany, pp.826–829

[14] Zhang K Q and Li D Z 2001 *Electromagnetic Theory for Microwaves and Optoelectronics*, 2nd edn. (Beijing: Publishing House of Electronics Industry) pp. 423–426

[15] Lu Z G, Gong Y B, Wei Y Y and Wang W X 2006 *Chin. Phys.* **15** 2661

[16] Mcvey B D Basten M A, Booske J H, Joe J and Scharer J E 1994 *IEEE Trans. Microwave Theory Technol.* **42** 995

[17] Mineo M and Paoloni C 2010 *IEEE Trans. Electron Dev.* **57** 1481

[18] Marshall E M, Walsh J E, Price E J and Jackson J A 1990 *Int. J. Infrared and Millimeter Waves* **11** 1189

[19] Paoloni C, Mineo M and Carlo A D 2011 *General Assembly and Scientific Symposium*, August 13–20, 2011, Istanbul, Turkey

[20] Zaginaylov G I, Gandel Y V, Kamyshan O P, Kamyshan V V, Hirata A, Thumvongskul T and Shiozawa T 2002 *IEEE Trans. Plasma Sci.* **30** 1151

[21] Milcho M V Yefimov B P Zavertanniy V V Goncharov V V 2016 *Telecommunications and Radio Engineering* **65** 719

[22] Nusinovich G S and Bliokh Y P 2000 *Phys. Plasmas* **7** 1294

[23] Li S, Wang J G, Teng Y, Wang G Q, Song Z M and Zeng P 2015 *The 16th IEEE International Vacuum Electronics Conference*, April 27–29, 2015, Beijing, China

[24] Vavriv D M 2008 *Telecommunications and Radio Engineering* **67** 751

[25] Vavriv D M 2006 *AIP Conf. Proc.* **807** 367

[26] Wang G Q, Wang J G, Lu X C, Li S and Zeng P 2015 *Chin. J. Vac. Sci. Technol.* **35** 1059

[27] Wang J G, Zhang D H, Liu C L, Li Y D, Wang Y, Wang H G, Qiao H L and Li X Z 2009 *Phys. Plasmas* **16** 033108

[28] Wang J G, Wang Y and Zhang D H 2006 *IEEE Trans. Plasma Sci.* **34** 681

[29] Wang J G, Chen Z G, Wang Y, Zhang D H, Liu C L, Li Y D, Wang H G, Qiao H L, Fu M Y and Yuan Y 2010 *Phys. Plasmas* **17** 073107